

pubs.acs.org/JACS Article

Tailoring Synthetic Polypeptide Design for Directed Fibril Superstructure Formation and Enhanced Hydrogel Properties

3 Tianjian Yang, Tianrui Xue, Jianan Mao, Yingying Chen, Huidi Tian, Arlene Bartolome, Hongwei Xia,

⁴ Xudong Yao, Challa V. Kumar, Jianjun Cheng,* and Yao Lin*



Cite This: https://doi.org/10.1021/jacs.3c10762



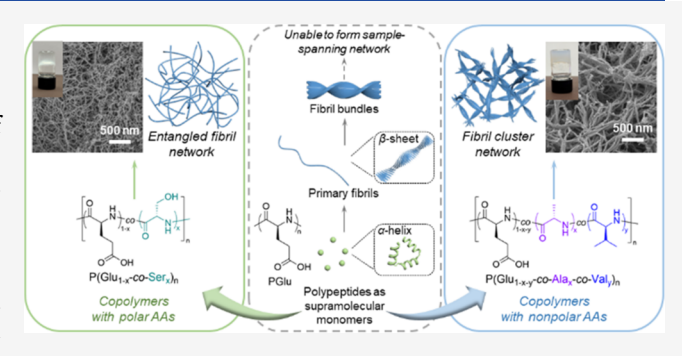
ACCESS

III Metrics & More

Article Recommendations

supporting Information

5 ABSTRACT: The biological significance of self-assembled protein 6 filament networks and their unique mechanical properties have 7 sparked interest in the development of synthetic filament networks 8 that mimic these attributes. Building on the recent advancement of 9 autoaccelerated ring-opening polymerization of amino acid N-10 carboxyanhydrides (NCAs), this study strategically explores a 11 series of random copolymers comprising multiple amino acids, 12 aiming to elucidate the core principles governing gelation pathways 13 of these purpose-designed copolypeptides. Utilizing glutamate 14 (Glu) as the primary component of copolypeptides, two targeted 15 pathways were pursued: first, achieving a fast fibrillation rate with 16 lower interaction potential using serine (Ser) as a comonomer,



17 facilitating the creation of homogeneous fibril networks; and second, creating more rigid networks of fibril clusters by incorporating 18 alanine (Ala) and valine (Val) as comonomers. The judicious selection of amino acids played a pivotal role in steering both the 19 morphology of fibril superstructures and their assembly kinetics, subsequently determining their potential to form sample-spanning 20 networks. Importantly, the viscoelastic properties of the resulting supramolecular hydrogels can be tailored according to the specific 21 copolypeptide composition through modulations in filament densities and lengths. The findings enhance our understanding of 22 directed self-assembly in high molecular weight synthetic copolypeptides, offering valuable insights for the development of synthetic 23 fibrous networks and biomimetic supramolecular materials with custom-designed properties.

24 INTRODUCTION

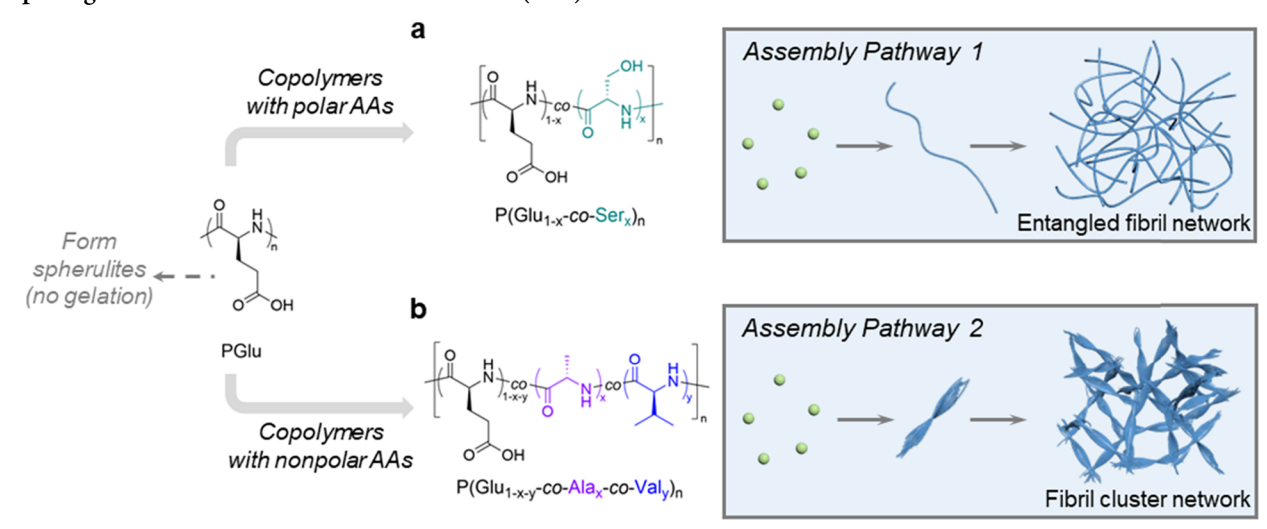
25 The self-assembly of semiflexible protein filaments into 26 networks through cross-linking or bundling is a ubiquitous 27 phenomenon in biology, with examples including the 28 cytoskeleton and collagen network. 1-6 The mechanical 29 properties of these filament networks hinge on the density of 30 cross-links and the physical attributes of individual filaments. 31 The interplay gives rise to distinct mechanical behaviors, such 32 as viscoelasticity and mechanical plasticity that are often absent 33 in synthetic polymeric gels. ^{7–15} Therefore, there is significant 34 interest in the design of synthetic filament networks that can 35 mimic the fibrillarity and viscoelastic properties of biological 36 gels. Specifically, materials derived from short peptides and 37 polypeptides, prepared by solid-phase synthesis or recombi-38 nant technology, along with their amphiphilic variants, have 39 greatly enhanced our understanding of the rational design of 40 synthetic filament networks with the desired macroscopic 41 properties. 16-29

42 High molecular weight (MW) synthetic polypeptides, 43 produced via the ring-opening polymerization (ROP) of 44 amino acid N-carboxyanhydride (NCA),^{30–34} have emerged 45 as another promising candidate for developing bioinspired 46 filament networks. Long regarded as model compounds for proteins, these polypeptides can be synthesized on a large 47 scale, making them cost-effective substitutes for biomaterial 48 applications. Remarkably, even homopolymers of a single type 49 of amino acid are capable of assembling into β -sheet 50 nanofibrils in aqueous solutions under appropriate pH and 51 temperature conditions. ^{35,36} However, many such "simple" 52 polypeptides either are incapable of forming supramolecular 53 hydrogels or can do so only under highly specific conditions. 54 To achieve successful hydrogel formation, rapid nanofibril 55 entanglement or linkage is essential to generate a cohesive, 56 sample-spanning network as opposed to precipitation. This 57 constraint restricts their broader application as viscoelastic 58 biomaterials. For example, under acidic conditions, poly($_{\rm L}$ - 59 glutamic acid) (PGlu) forms amyloid-like fibrils that bundle 60 into twisted ribbons. ^{36–38} This transformation is driven by the 61 thermodynamic tendency for aggregated fibrils to adopt 62

Received: September 29, 2023 Revised: December 16, 2023 Accepted: December 18, 2023



Scheme 1. Illustration of the Two Supramolecular Hydrogelation Pathways Using Synthetic Random Copolypeptides Comprising Two or Three Different Amino Acids (AAs)



^a(a) Pathway 1 focuses on reducing fibril interaction potential, leading to a network of entangled long fibrils. (b) Pathway 2 centers on coupling enhanced β -sheet formation propensity with hydrophobicity, producing sample-spanning networks defined by interconnected fibril clusters.

63 pairwise orientation. Instead of progressing to gel states, these 64 fibrils often crystallize into spherulite microparticles and 65 precipitate.

Our aim is to elucidate the fundamental principles governing 67 the networking pathways from nanofibrils of diverse inter-68 action strengths and complex superstructures, diverging from 69 the commonly employed amphiphilic assembly strategies. 39,40 70 Gel formation, driven by the attractive forces between 71 nanofibrils in concentrated suspension and subsequent 72 percolation transitions, is an intricate nonequilibrium proc-73 ess. 41-44 This process is shaped by an array of fibril 74 characteristics, such as their aspect ratio, flexibility, tendency 75 to bundle, entangle, or cross-link as well as the dynamics of 76 fibril clustering and cross-link formation. 41,45-49' Realizing 77 sample-spanning networks with the desired mechanical 78 properties demands extensive tunability of these parameters. 79 In the realm of synthetic polypeptides, a promising tactic to 80 address this challenge involves creating random copolymers 81 that incorporate two or more distinct amino acids within single 82 chains. The approach grants control over the self-assembly 83 process, fibril properties, and network formation by adjusting 84 the composition of copolypeptides. Given the vast chemical 85 landscape provided by the 20 canonical amino acids, along 86 with numerous unnatural amino acids, 32,50,51 we can explore a 87 diverse array of synthetic copolypeptides for the development 88 of supramolecular hydrogels with tailored structures and 89 properties.

Herein, we demonstrate that while certain homopolypep-91 tides might be unable to form hydrogels on their own, their 92 integration with other amino acids in random copolymers can 93 lead to the development of supramolecular hydrogels with 94 diverse fibril superstructures and mechanical properties. We 95 selected glutamic acid (Glu) as the primary amino acid 96 component in the copolymers given that PGlu itself cannot 97 form a gel. We evaluated how the addition of one or two extra 98 amino acids as comonomers, such as serine (Ser), leucine 99 (Leu), valine (Val), tyrosine (Tyr), or alanine (Ala), could 100 alter the fibril superstructure and gelation behavior of the 101 copolypeptides. The recent advancement of autoaccelerated, 102 cooperative covalent polymerization of NCAs has made it possible to incorporate widely different amino acids in random 103 copolymers while maintaining good control over the chemical 104 composition and MWs. 52-54 The process even accommodates 105 amino acids like Ser, Val, and Tyr, which have a propensity to 106 form β -sheets and are typically challenging to integrate using 107 conventional methods. 55-58 Leveraging this advanced techni- 108 que, we successfully identified two distinct pathways that lead 109 to supramolecular gelation of these random copolypeptides. 110

In the first approach, we designed the copolypeptide to have 111 a fast fibrillation rate but a lower interaction potential among 112 the formed fibrils. This allowed fibrils to remain relatively 113 stable in suspension and entangle into homogeneous fibril 114 networks at sufficiently high concentrations. Ser was found to 115 be effective in facilitating supramolecular gelation over a broad 116 composition range of the $P(Glu_{1-x}-co-Ser_x)_n$ copolymers 117 (Scheme 1a), where n denotes the degree of polymerization 118 s1 (DP) and x and 1 - x denote the percentage composition of 119 Ser and Glu, respectively. In the second approach, we explored 120 the possibility of generating networks of branched fibril 121 clusters by increasing the connectivity between the fibrils. 122 Copolymers of Glu, Ala, and Val, $P(Glu_{1-x-y}-co-Ala_x-co-Val_y)_n$ 123 (Scheme 1b), where x and y denote the percentage 124 composition of Ala and Val, respectively, were found to form 125 branched fibril clusters. Gelation occurred when the dynamics 126 of the fibril clusters were arrested with network connectivity at 127 appropriate concentrations. Fibril networks resulting from both 128 pathways exhibited rheological properties of supramolecular 129 gels, with considerable tunability in viscoelastic properties 130 observed upon varying the composition of the copolypeptides. 131

■ RESULTS AND DISCUSSION

Synthesis of Diverse Copolypeptides as Supra- 133 molecular Monomers. We have designed a series of 134 copolypeptides as supramolecular monomers with different 135 compositions through the controlled ROP of NCAs. All of the 136 NCA monomers we used in the study can be synthesized with 137 high purity and scaled up effectively for copolymerization. The 138 $P(Glu_{1-x}-co-Ser_x)_n$ copolymers were synthesized using the 139 SIMPLE (Segregation-Induced Monomer-Purification and 140

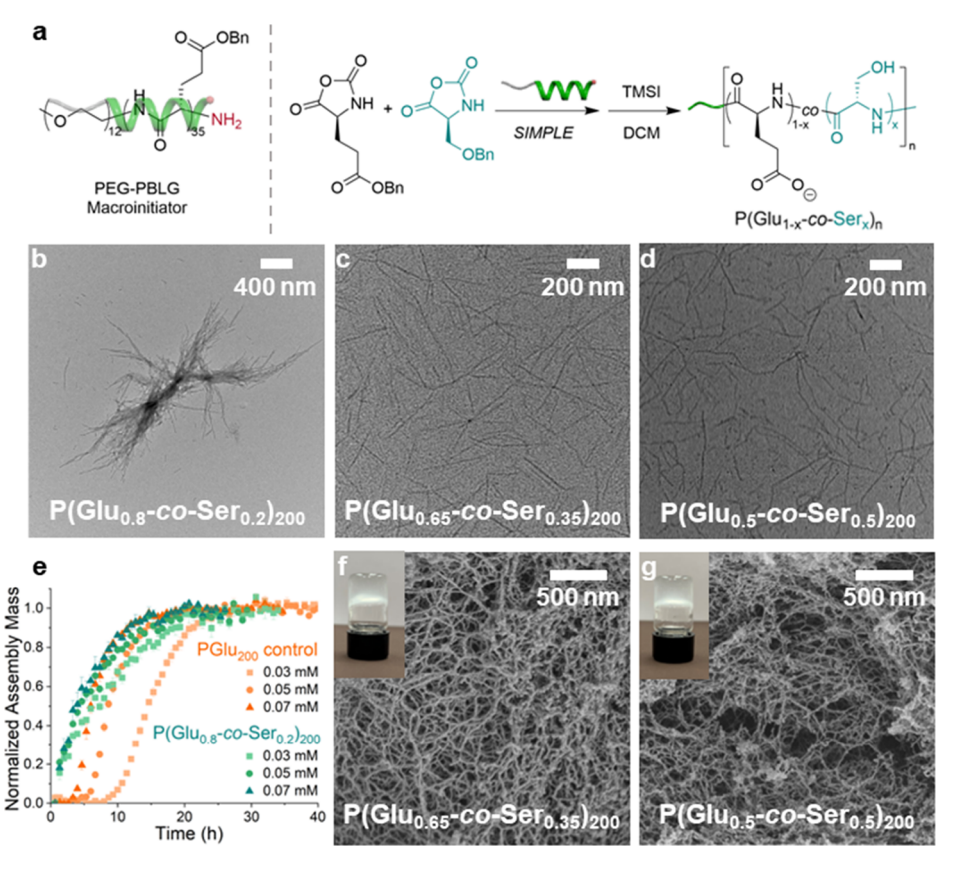


Figure 1. Synthesis and supramolecular assembly of $P(Glu_{1-x}\text{-}co\text{-}Ser_x)_n$ into long fibrils and entangled fibril networks. (a) Synthetic route of $P(Glu_{1-x}\text{-}co\text{-}Ser_x)_n$. (b) TEM image of the fibril bundles from $P(Glu_{0.85}\text{-}co\text{-}Ser_{0.2})_{200}$. (c, d) TEM images of the dispersed fibrils from $P(Glu_{0.65}\text{-}co\text{-}Ser_{0.35})_{200}$ and $P(Glu_{0.5}\text{-}co\text{-}Ser_{0.5})_{200}$, respectively. (e) Kinetic assembly profiles for $P(Glu_{0.05}\text{-}co\text{-}Ser_{0.2})_{200}$ (in green) across different initial monomer concentrations. (f, g) SEM images of the entangled fibril networks from supercritical $P(Glu_{0.65}\text{-}co\text{-}Ser_{0.35})_{200}$ and $P(Glu_{0.5}\text{-}co\text{-}Ser_{0.5})_{200}$, respectively. Inset: photographs of their translucent supramolecular hydrogels were taken at a concentration of 20 mg/mL.

141 initiator-Localization promoted rate-Enhancement) polymer-142 ization method initiated by the macroinitiator followed by 143 iodotrimethylsilane (TMSI) deprotection. 53,59 The P(Glu_{1-x}- $_{144}$ co-Leu_x)_n and P(Glu_{1-x}-co-Ala_x)_n copolymers were synthesized 145 from the DMF phase using hexylamine as the initiator using 146 previously reported methods, followed by TMSI deprotec-147 tion. The $P(Glu_{1-x}$ -co- $Val_x)_n$ and $P(Glu_{1-x}$ -co- $Tyr_x)_n$ copolymers were synthesized from DCM phase using hexylamine as 149 initiator using previously reported methods, followed by TMSI 150 deprotection. The P(Glu_{1-x-y}-co-Ala_x-co-Val_y)_n copolymers 151 were synthesized from crown ether (CE) catalyzed polymer-152 ization method, followed by TMSI deprotection. 63 All the copolymers have similar degree of polymerization (DP ~ 100 154 or 200), low polydispersity (D < 1.1), and precise composition 155 control. Detailed synthesis and characterization of the 156 corresponding macromolecules are shown in the Supporting 157 Information (Figures S2-8, Table S1, and Figure S35-49).

Exploring the Role of Serine in the Rapid Formation of Entangled Fibril Networks. We first focused on developing long fibrils from copolypeptides that remain stable when diluted but transition into entangled fibril networks as the concentration increases. Serine (Ser) was selected owing to distinct polar side chains and its propensity toward β-sheet formation. This exploration into entangled fibril network was motivated by the observed gelation characteristics of poly($_{L^{-}}$ 166 lysine) (PLys). Unlike PGlu and most homopolypeptides, Plys can transform into hydrogels, consisting of elongated nano-

fibrils, when the side-chain charges neutralize under alkaline 168 conditions (Figure S1). This transformation is notably rapid 169 and devoid of the typical nucleation lag phases often seen in 170 amyloid-like supramolecular assemblies. The Given Ser's 171 propensity for β -sheet structures and its increased 172 hydrophilicity compared to Glu in acidic environments where self-assembly occurs, it is anticipated to act as a catalyst 174 in the formation of widespread, elongated fibrils. At sufficiently 175 high concentrations, these copolypeptide fibrils are likely to 176 intertwine swiftly to form a sample-spanning network, 177 overcoming the stacking challenges of PGlu fibrils and offering 178 a cohesive and stable hydrogel structure, circumventing 179 precipitation constraints.

We synthesized three $P(Glu_{1-x}\text{-}co\text{-}Ser_x)_{200}$ samples with 181 increasing percentages of Ser (x=0.2, 0.35 and 0.5) using 182 autoaccelerated ROP-NCA in a water/dichloromethane 183 (DCM) biphasic system with macroinitiators (SIMPLE 184 polymerization), according to the procedures reported 185 previously 53,59 (Figure 1a and Figure S2-3). The statistical 186 fi randomness of Glu and Ser incorporation into the copolymer 187 chains was confirmed by monitoring the monomers con-188 sumption kinetics during the copolymerization (Figure S9). 189 The copolypeptides, similar to PGlu, experienced a con-190 formation shift from coil to helix when the pH was decreased 191 from neutral to acidic, resulting in the suppression of 192 carboxylate ionization (Figure S10). Under mild heating 193 conditions that destabilize α -helixes, aggregated β -structures 194

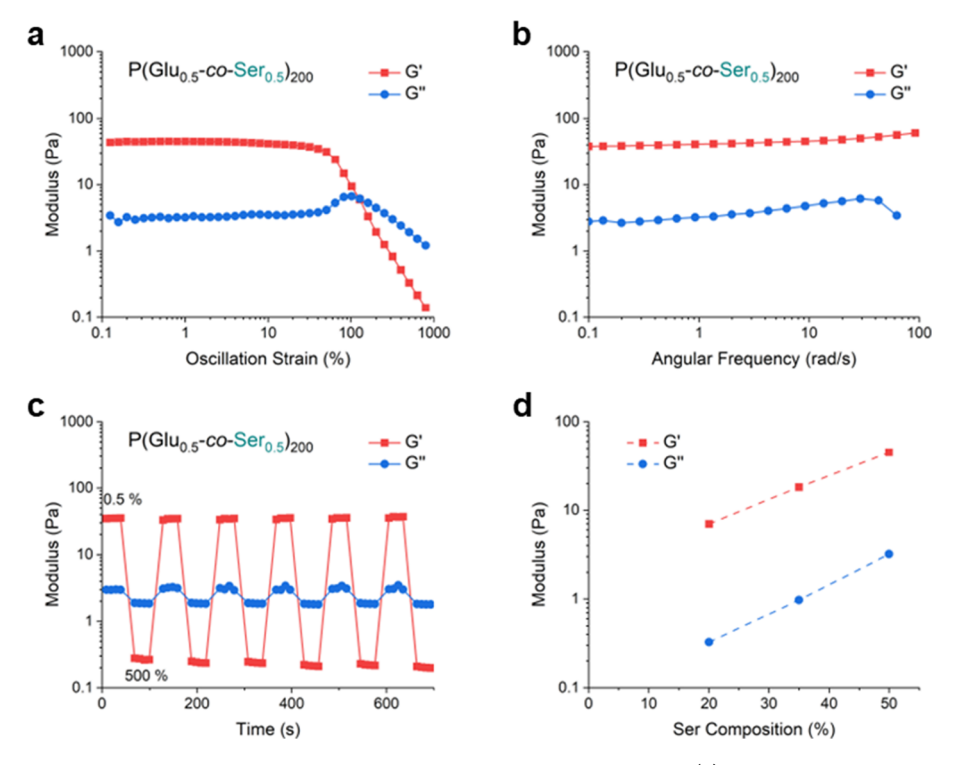


Figure 2. Rheological characteristics of hydrogel networks of entangled copolypeptide fibrils. (a) Strain-dependent oscillatory rheology for the $P(Glu_{0.5}$ -co-Ser_{0.5})₂₀₀ hydrogel, conducted at ω = 1.0 rad/s and 25 °C. (b) Frequency-dependent oscillatory rheology for the $P(Glu_{0.5}$ -co-Ser_{0.5})₂₀₀ hydrogel under 0.5% strain at 25 °C. (c) Oscillatory rheology $P(Glu_{0.5}$ -co-Ser_{0.5})₂₀₀ hydrogel showcasing self-healing properties when alternated between 0.5 and 500% strain over 30-s intervals at ω = 1.0 rad/s and 25 °C. (d) Comparison of storage and loss modulus for $P(Glu_{1-x}$ -co-Ser_x)₂₀₀ supramolecular networks based on varying Ser compositions in the copolymer, measured under 1.0% strain, ω = 1.0 rad/s, and 25 °C. Polymer concentration is maintained at 20 mg/mL.

195 typically form as they maximize local contacts, rendering them 196 thermodynamically more stable than α -helices. We selected the 197 fibrillation condition of pH 4.0 and 45 °C, commonly used in 198 previous studies, $^{36-38}$ to investigate the impact of varying Ser 199 compositions on the fibrillation process.

The transmission electron microscopy (TEM) images 200 201 presented in Figure 1b-d illustrate the fibril morphology 202 from three $P(Glu_x-co-Ser_{1-x})_{200}$ samples, prepared in water 203 with the pH adjusted to 4 using HCl. At a Ser content of 20%, 204 P(Glu_{0.8}-co-Ser_{0.2})₂₀₀ formed loose fibril bundles (Figure 1b), 205 which were distinct from tightly stacked, ribbon-like structure 206 assembled from PGlu (Figure S1). The introduction of more 207 hydrophilic Ser in the copolypeptide lowered the interaction potential among the formed fibrils, resulting in fibrils with a less tendency to assume pairwise orientation. As the Ser 210 content reached 35% or 50%, most fibrils remained 211 individually dispersed, with an average width of ~10 nm and length of hundreds of nanometers (Figure 1c,d). Fourier-213 transform infrared spectra (FTIR) and wide-angle X-ray diffraction (WAXD) of the fibrils revealed that they were 215 primarily composed of β -sheet structures (Figure S16 and 216 S17). The kinetics of fibrillation were examined using 217 thioflavin T (ThT)^{37,70} in a 15 mM acetate buffer (pH 4), 218 monitoring the enhanced fluorescence emission upon ThT's 219 binding to β -sheet structures. TEM analysis confirmed that the 220 fibril morphologies remained consistent in the presence of an acetate buffer (as shown in Figure S23). Unlike the slow, 222 nucleation-controlled assembly of PGlu, the copolypeptides, 223 such as P(Glu_{0.8}-co-Ser_{0.2})₂₀₀ even in diluted solutions, 224 displayed no initial lag phase—a stage typically marked by 225 slow nucleation prior to rapid fibril growth—as shown in Figure

1e. The kinetic rate of fibrillation accelerated with an 226 increasing Ser percentage (Figure S22), attributable to the 227 reduced charge repulsion and enhanced β -sheet propensity 228 within the copolymers.

At a more concentrated solution (e.g., 20 mg/mL), $P(Glu_{0.8}^{-} 230 co-Ser_{0.2})_{200}$ remained as fibril suspensions. In contrast, 231 $P(Glu_{0.65}\text{-}co-Ser_{0.35})_{200}$ and $P(Glu_{0.5}\text{-}co-Ser_{0.5})_{200}$ formed hydro- 232 gels within 30 min (insets of Figure 1f,g). The scanning 233 electron microscopy (SEM) images showed that the hydrogels 234 of both samples were made of an entangled supramolecular 235 fibril network (Figure 1f,g). The fibrils in the networks had a 236 similar width as the dispersed fibrils found in the diluted 237 suspension. The viscoelastic properties of these supramolecular 238 gels were then characterized by shear rheology.

Assessing and Tuning the Mechanical Properties of 240 $P(Glu_{1-x}-co-Ser_x)_{200}$ Hydrogels. We examined the storage 241 modulus (G') and loss modulus (G'') as functions of 242 oscillatory strain and frequency for the P(Glu_{0.5}-co-Ser_{0.5})₂₀₀ 243 hydrogels, as shown in Figure 2a-c. Within these hydrogels, 244 f2 G' was substantially higher than G'', and negligible frequency 245 dependence was observed, thus indicating their predominantly 246 elastic nature. Figure 2a shows the results of the strain- 247 dependent oscillatory rheology. The hydrogel made from 248 $P(Glu_{0.5}$ -co-Ser_{0.5})₂₀₀ demonstrated a G' of 40 Pa and sustained 249 this value up to strains nearing ~50%. Remarkably, in step- 250 strain experiments—where a high strain (500%) was 251 introduced after a low strain (0.5%) to perturb the hydrogel 252 network and followed by another low strain to assess the 253 network's recovery—this hydrogel demonstrated impressive 254 self-healing abilities (Figure 2c). The G' of P(Glu_{0.5}-co- 255 Ser_{0.5})₂₀₀ returned to approximately 100% of its initial value 256

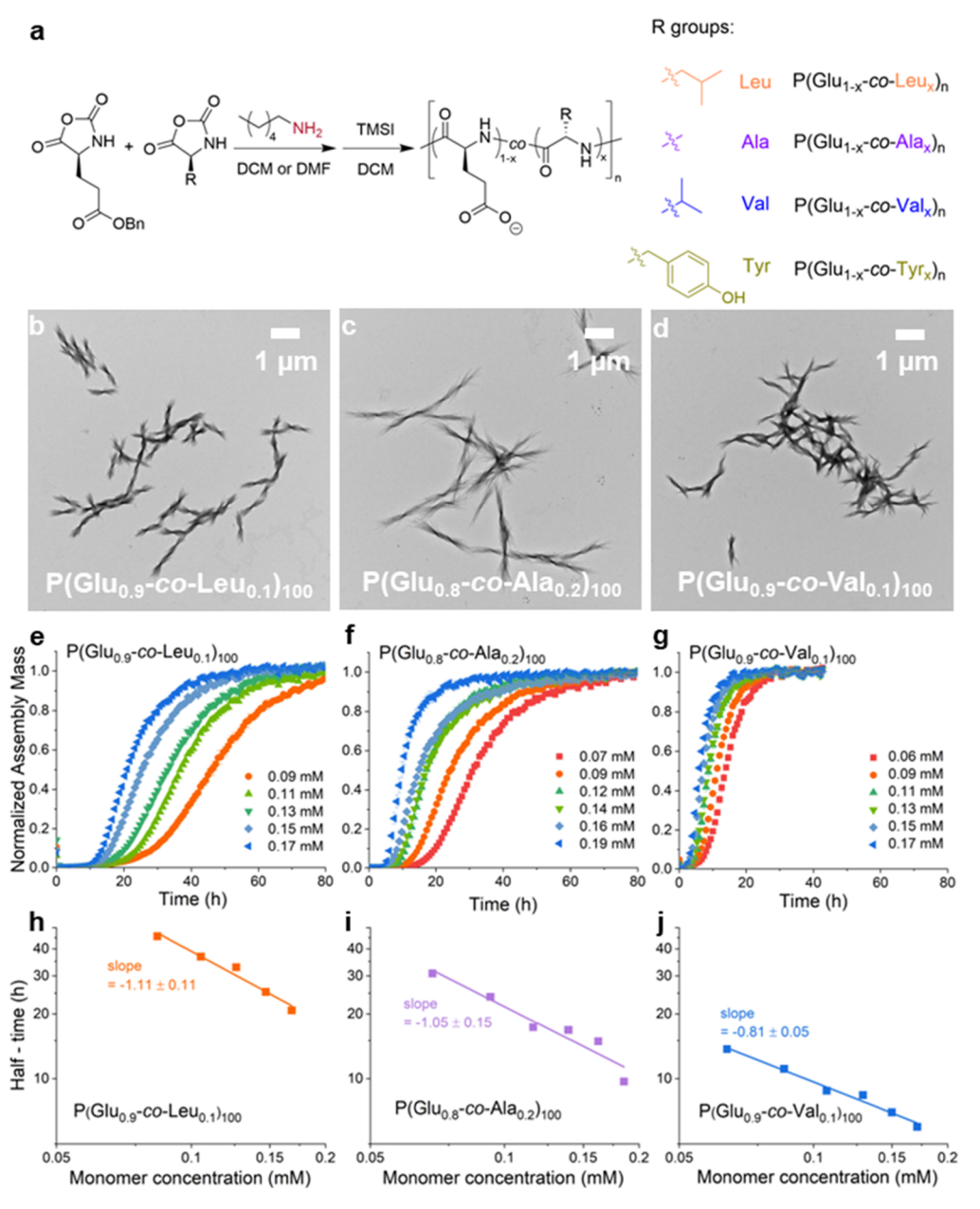


Figure 3. Supramolecular assembly of bicomponent random copolypeptides incorporating hydrophobic secondary amino acids. (a) Schematic representation of the synthetic routes of $P(Glu_{1-x}\text{-}co\text{-}Leu_x)_n$, $P(Glu_{1-x}\text{-}co\text{-}Ala_x)_n$, $P(Glu_{1-x}\text{-}co\text{-}Val_x)_n$, and $P(Glu_{1-x}\text{-}co\text{-}Tyr_x)_n$. (b-d) TEM images of the supramolecular fibril clusters for $P(Glu_{0.9}\text{-}co\text{-}Leu_{0.1})_{100}$, $P(Glu_{0.8}\text{-}co\text{-}Ala_{0.2})_{100}$, and $P(Glu_{0.9}\text{-}co\text{-}Val_{0.1})_{100}$, respectively. (e-g) Assembly kinetic profiles for $P(Glu_{0.9}\text{-}co\text{-}Leu_{0.1})_{100}$, $P(Glu_{0.8}\text{-}co\text{-}Ala_{0.2})_{100}$, and $P(Glu_{0.9}\text{-}co\text{-}Val_{0.1})_{100}$, respectively, across a range of initial monomer concentrations. (h-j) Power-law scaling of the time to half-completion $(t_{1/2})$ as a function of the initial monomer concentration during the assembly of $P(Glu_{0.9}\text{-}co\text{-}Leu_{0.1})_{100}$, $P(Glu_{0.8}\text{-}co\text{-}Ala_{0.2})_{100}$, and $P(Glu_{0.9}\text{-}co\text{-}Val_{0.1})_{100}$, respectively. Data points (represented by solid squares) were subjected to linear regression analysis (depicted by solid lines) to determine the slope that corresponds to the scaling exponent.

 $_{257}$ within seconds after the removal of high strain. By varying the $_{258}$ Ser composition, we can tune the hydrogel's properties. For $_{259}$ instance, the supramolecular hydrogel produced from P- $_{260}$ (Glu_{0.65}- $_{co}$ -Ser_{0.35})₂₀₀ (Figure S32) exhibited a softer gel $_{261}$ compared to the P(Glu_{0.5}- $_{co}$ -Ser_{0.5})₂₀₀. Conversely, P(Glu_{0.8}- $_{262}$ $_{co}$ -Ser_{0.2})₂₀₀ resulted in a viscous solution (Figure S31). The $_{263}$ comparison among the three variants is showcased in Figure 264 2d.

While the $P(Glu_{1-x}$ -co- $Ser_x)_{200}$ samples exemplify the tunable and reversible nature of supramolecular gels based 267 on the entanglement of elongated dispersed fibrils, such 268 dynamic attributes may also compromise their mechanical

robustness. To address this, we subsequently pursued a $_{269}$ strategy to bolster the noncovalent network connections by $_{270}$ incorporating nonpolar amino acids known for their strong β - $_{271}$ sheet-forming propensity into the copolypeptides. This $_{272}$ modification gives rise to superstructures of stiff, branched $_{273}$ fibril clusters that can rapidly coalesce into a cohesive, sample- $_{274}$ spanning network, thereby offering the potential for enhanced $_{275}$ mechanical strength.

Diversifying Fibril Superstructures with Hydrophobic 2777 **Amino Acid Integration.** We utilized the ROP of NCA to 278 synthesize a diverse set of copolypeptides, with Glu as the 279 primary component and varying amounts of Leu, Val, Ala, or 280

Figure 4. Supramolecular assembly and fibril network of tricomponent copolypeptides $P(Glu_{1-x-y}\text{-}co\text{-}Ala_x\text{-}co\text{-}Val_y)_n$. (a) Schematic representation of the synthetic route for $P(Glu_{1-x-y}\text{-}co\text{-}Ala_x\text{-}co\text{-}Val_y)_n$. (b, e) Kinetic assembly profiles for $P(Glu_{0.65}\text{-}co\text{-}Ala_{0.3}\text{-}co\text{-}Val_{0.05})_{200}$ and $P(Glu_{0.7}\text{-}co\text{-}Ala_{0.2}\text{-}co\text{-}Val_{0.1})_{200}$, respectively, at various initial monomer concentrations. (c, f) TEM images of assemblies from $P(Glu_{0.65}\text{-}co\text{-}Ala_{0.3}\text{-}co\text{-}Val_{0.05})_{200}$ and $P(Glu_{0.7}\text{-}co\text{-}Ala_{0.2}\text{-}co\text{-}Val_{0.1})_{200}$, respectively. (d, g) SEM images of $P(Glu_{0.65}\text{-}co\text{-}Ala_{0.3}\text{-}co\text{-}Val_{0.05})_{200}$ and $P(Glu_{0.7}\text{-}co\text{-}Ala_{0.2}\text{-}co\text{-}Val_{0.1})_{200}$ hydrogels, respectively, after supercritical $P(Clu_{0.65}\text{-}co\text{-}Ala_{0.2}\text{-}co\text{-}Val_{0.1})_{200}$ in the opaque supramolecular hydrogels concentrated at 20 mg/mL.

281 Tyr. Among these amino acids, Val, Ala, and Tyr have a notable β -sheet propensity. For contrast, Leu, known for its propensity to form stable α -helical conformation, was also integrated. 66-68 Our synthesized series includes P(Glu_{1-x}-co- Leu_{x})₁₀₀, $P(\text{Glu}_{1-x}\text{-}co\text{-}\text{Ala}_{x})_{100}$, $P(\text{Glu}_{1-x}\text{-}co\text{-}\text{Val}_{x})_{100}$, and P- $(Glu_x-co-Tyr_{1-x})_{n}$, with 'x' values ranging between 0.05 to 0.4 (Figure 3a and Figure S4-7). Conformations of the resulting copolypeptides at different pH values were confirmed by CD (Figure S11-14). Given the pronounced hydrophobicity of Leu 290 and Val's side chains, ⁶⁹ copolypeptides consisting of more than 291 15% of these amino acids rapidly segregated into amorphous 292 structures under the assembly conditions. However, both $P(Glu_{0.9}-co-Leu_{0.1})_{100}$ and $P(Glu_{0.9}-co-Val_{0.1})_{100}$ formed distinct 294 fibril superstructures in the diluted solutions (Figure 3b,d, 295 Figure S25 and S27). Individual fibrils in the bundles can be visualized in the negative stained TEM images (Figure S24). In comparison, $P(Glu_{1-x}-co-Ala_x)_{100}$, with Ala compositions of 298 20% or 30%, produced fibril superstructures (Figure 3c and 299 Figure S26), attributed to the slightly reduced hydrophobic nature of Ala's side chain compared to Leu or Val. These 301 fibrils, especially from P(Glu_{0.9}-co-Leu_{0.1})₁₀₀ and P(Glu_{0.9}-co- $Val_{0,1}$)₁₀₀, predominantly exhibited a β -sheet secondary structure, as revealed by FTIR and WAXD studies (Figure 304 S18 and S19). In addition to the β -sheet structure, coil 305 conformation was also evident in fibrils from P(Glu_{0.8}-co-306 Ala_{0.2})₁₀₀, with FITR spectra indicating a peak at 1645 cm⁻¹ 307 and WAXD profiles lacking the α -helix signature (Figure S18 308 and S19). In contrast, $P(Glu_x-co-Tyr_{1-x})_n$ primarily formed

amorphous aggregates in solution, as a result of the strong 309 interactions between aromatic side groups (Figure S28).

P(Glu_{0.9}-co-Leu_{0.1})₁₀₀ demonstrated the slowest fibril for- 311 mation, with the fibrillation following a two-stage, nucleation- 312 growth process that could be accelerated by increasing the 313 polymer concentration (Figure 3e and Figure S25). The 314 kinetics was even slower than that of PGlu, as Leu has a high 315 propensity to form a α -helical conformation, trapping the 316 copolypeptides in the helical state before they convert into β - 317 sheet fibrils. The slowly formed fibrils assembled pairwise into 318 well-ordered bundles, and gelation was not observed, even at 319 saturated concentrations. Ala, considered to be equally adept in 320 forming α -helical and β -sheet structures, ^{71,72} influences the ₃₂₁ fibrillation of P(Glu_{0.8}-co-Ala_{0.2})₁₀₀ differently. As shown in 322 Figure 3f and Figure S26, this copolypeptide fibrillated faster 323 than $P(Glu_{0.9}$ -co-Leu_{0.1})₁₀₀. The resultant fibrils from $P(Glu_{0.8}$ - 324 $(co-Ala_{0.2})_{100}$ exhibit a combination of β -sheet and coil 325 structures. Interestingly, the fibrils in the superstructures 326 were considerably loose, presumably because the higher 327 percentage of Ala disrupted the regularity of the fibril 328 interactions. In diluted conditions, the fibrils measured a few 329 microns in length and became even longer when the Ala 330 composition in the copolypeptides increased from 20% to 30% 331 (Figure S26f). However, no gelation was observed, although 332 the suspension became viscous at high polymer concentrations. 333 Val has the strongest β -sheet propensity among the nonpolar 334 amino acids we tested.^{66–68} Similar to Ser, there was almost no 335 lag phase in the fibrillation of $P(Glu_{0.9}$ -co- $Val_{0.1})_{100}$ (Figure 3g 336

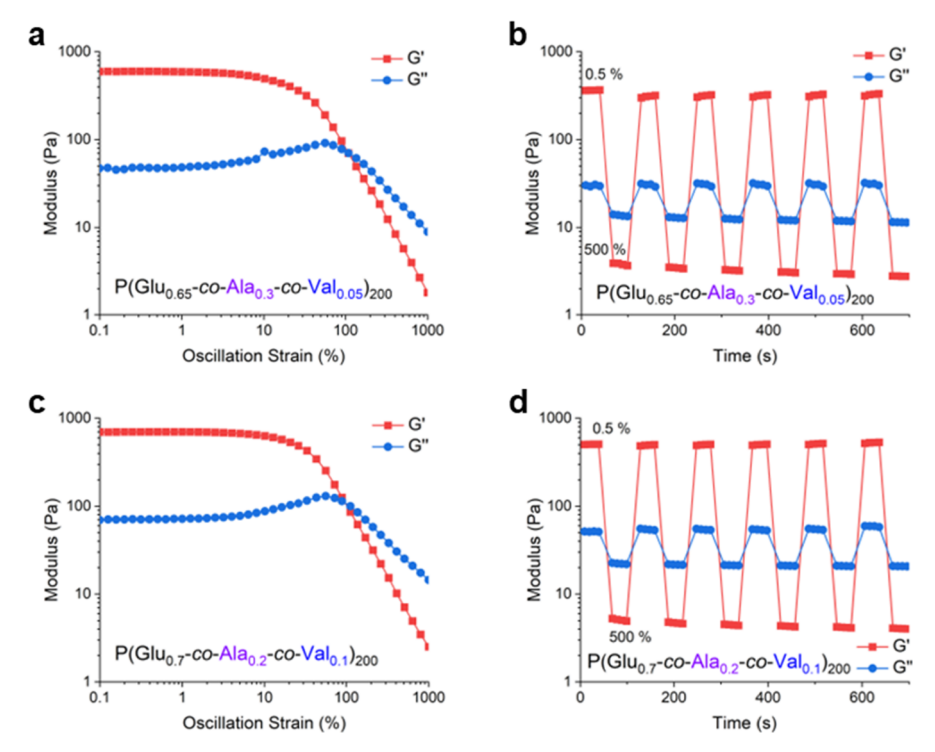


Figure 5. Rheological behavior of hydrogel networks comprising interlinked fibril clusters. (a, c) Strain-dependent oscillatory rheology ($\omega = 1.0$ $rad/s, 25 \ ^{\circ}C) \ for \ P(Glu_{0.65}\text{-}co\text{-}Ala_{0.3}\text{-}co\text{-}Val_{0.05})_{200} \ and \ P(Glu_{0.7}\text{-}co\text{-}Ala_{0.2}\text{-}co\text{-}Val_{0.1})_{200} \ hydrogel, \ respectively. \ (b, \ d) \ Oscillatory \ rheology \ of \ P(Glu_{0.65}\text{-}co\text{-}Ala_{0.2}\text{-}co\text{-}Val_{0.1})_{200} \ hydrogel, \ respectively. \ (b, \ d) \ Oscillatory \ rheology \ of \ P(Glu_{0.65}\text{-}co\text{-}Ala_{0.2}\text{-}co\text{-}Val_{0.1})_{200} \ hydrogel, \ respectively. \ (b, \ d) \ Oscillatory \ rheology \ of \ P(Glu_{0.65}\text{-}co\text{-}Ala_{0.2}\text{-}co\text{-}Val_{0.1})_{200} \ hydrogel, \ respectively. \ (b, \ d) \ Oscillatory \ rheology \ of \ P(Glu_{0.65}\text{-}co\text{-}Ala_{0.2}\text{-}co\text{-}Val_{0.1})_{200} \ hydrogel, \ respectively. \ (b, \ d) \ Oscillatory \ rheology \ of \ P(Glu_{0.65}\text{-}co\text{-}Ala_{0.2}\text{-}co\text{-}Val_{0.1})_{200} \ hydrogel, \ respectively. \ (b, \ d) \ Oscillatory \ rheology \ of \ P(Glu_{0.65}\text{-}co\text{-}Ala_{0.2}\text{-}co\text{-}Val_{0.1})_{200} \ hydrogel, \ respectively. \ (b, \ d) \ Oscillatory \ rheology \ of \ P(Glu_{0.65}\text{-}co\text{-}Ala_{0.2}\text{-}co\text{-}Val_{0.1})_{200} \ hydrogel, \ respectively. \ (b, \ d) \ Oscillatory \ rheology \ of \ P(Glu_{0.65}\text{-}co\text{-}Val_{0.1})_{200} \ hydrogel, \ respectively. \ (b, \ d) \ Oscillatory \ rheology \ of \ P(Glu_{0.65}\text{-}co\text{-}Val_{0.1})_{200} \ hydrogel, \ respectively. \ (b, \ d) \ Oscillatory \ rheology \ of \ P(Glu_{0.65}\text{-}co\text{-}Val_{0.1})_{200} \ hydrogel, \ respectively. \ (b, \ d) \ Oscillatory \ rheology \ of \ P(Glu_{0.65}\text{-}co\text{-}Val_{0.1})_{200} \ hydrogel, \ respectively. \ (b, \ d) \ Oscillatory \ rheology \ of \ P(Glu_{0.65}\text{-}co\text{-}Val_{0.1})_{200} \ hydrogel, \ respectively. \ (b, \ d) \ Oscillatory \ rheology \ of \ P(Glu_{0.65}\text{-}co\text{-}Val_{0.1})_{200} \ hydrogel, \ respectively. \ (b, \ d) \ Oscillatory \ rheology \ of \ P(Glu_{0.65}\text{-}co\text{-}Val_{0.1})_{200} \ hydrogel, \ respectively. \ (b, \ d) \ Oscillatory \ rheology \ of \ P(Glu_{0.65}\text{-}co\text{-}Val_{0.1})_{200} \ hydrogel, \ respectively. \ (b, \ d) \ Oscillatory \ rheology \ of \ P(Glu_{0.65}\text{-}co\text{-}Val_{0.1})_{200}$ co-Ala_{0.3}-co-Val_{0.05})₂₀₀ and P(Glu_{0.7}-co-Ala_{0.2}-co-Val_{0.1})₂₀₀ hydrogel, respectively, alternating between 0.5 and 500% strain over 30-s intervals (ω = 1.0 rad/s, 25 °C), demonstrating their self-healing characteristics. Concentration for P(Glu_{1-x-v} co-Ala_x-co-Val_v)₂₀₀ was set at 20 mg/mL.

337 and Figure S27). Due to the high hydrophobicity of Val, the 338 fibrils formed branched fibril clusters with multiple filaments at 339 a cross-link, but these connected clusters also tended to 340 precipitate under concentrated conditions.

The assembly kinetics were analyzed using established 342 models for protein and amyloid aggregation. ^{1,73,74} The time to 343 reach half-completion of fibril assembly (half-time) was 344 determined from the kinetic curves presented in Figure 3e-345 g. The scaling exponent (γ) , which indicates how the half-time 346 varies with the initial copolypeptide concentration, was derived 347 from the slopes in Figure 3h-j. The values of these exponents, 348 ranging from 0.8 to 1.4, suggest that secondary nucleation is 349 the predominant mechanism in fibril formation, similar to the 350 aggregation of amyloid- β peptides. 75,76 The initial growth 351 phase, as well as the entire assembly process, is well-described 352 by a fibril formation model that assumes control by secondary nucleation, with n_2 (the secondary nucleation reaction order with respect to the monomer) being 1, and n_c (the primary 354 355 nucleation reaction order) being 2 or 3, as detailed in Table S2 356 and Figure S30. Notably, the inclusion of Val in the copolypeptides markedly accelerates both primary and secondary nucleation, thus identifying Val as a potent modulator in the design of a tricomponent system. 359

To form a stable filament network, semiflexible filaments 360 361 must exceed a certain density and length for effective percolation through sufficient cross-linking. Moreover, cross-363 linking must occur rapidly to prevent large filament clusters 364 from precipitating out of the solution. Clearly, the distinct 365 nonpolar amino acids integrated into the copolypeptides 366 significantly influenced both the structural morphology and 367 connectivity of the fibril superstructures, as well as the kinetics 368 of their formation. To achieve an effective, sample-spanning 369 network, it is crucial to engineer fibril clusters with both high

aspect ratios and robust cross-linking propensities, while also 370 ensuring rapid kinetics throughout the assembly process. With 371 these criteria in mind, we proposed to combine Ala's fibril- 372 elongating effects with Val's rapid nucleation capabilities to 373 design $P(Glu_{1-x-v}$ -co-Ala_x-co-Val_v)_n copolypeptides for realizing 374 the formation of supramolecular filament network.

Tricomponent Copolypeptide Assembly into Rigid 376 Branched Fibril Networks. Leveraging on the crown-ether 377 (CE) catalyzed ROP-NCA method we recently developed, 63 378 we synthesized two samples, P(Glu_{0.65}-co-Ala_{0.3}-co-Val_{0.05})₂₀₀ 379 and P(Glu_{0.7}-co-Ala_{0.2}-co-Val_{0.1})₂₀₀, for examination (Figure 4a 380 f4 and Figure S8). Conformations of the resulting copolypeptide 381 at different pH values were confirmed by CD (Figure S15). 382 Under diluted conditions, both copolypeptides assembled into 383 loose, high-aspect-ratio fibril clusters without experiencing a 384 significant lag phase (Figure 4b,e). Those fibril clusters (Figure 385 4c,f) were much smaller than those from $P(Glu_{0.9}$ -co-Leu_{0.1})₁₀₀, 386 $P(Glu_{0.8}$ -co-Ala_{0.2})₁₀₀, and $P(Glu_{0.9}$ -co-Val_{0.1})₁₀₀ (Figure 3b-d). 387 When P(Glu_{0.65}-co-Ala_{0.3}-co-Val_{0.05})₂₀₀ was compared with 388 $P(Glu_{0.7}$ -co- $Ala_{0.2}$ -co- $Val_{0.1})_{200}$, the fibrillation process of the 389 latter markedly accelerated. This is presumably due to 390 increased nucleation sites prompted by the higher Val 391 composition, leading to thinner and shorter fibril clusters. In 392 concentrated solutions, supramolecular gelation occurred, 393 forming an intertwined filament network that manifested as 394 an opaque hydrogel (Figure 4d,g). The fibrils within these 395 networks shared a similar width with the fibril clusters found in 396 the diluted suspension. Unlike the entangled fibril networks 397 formed by $P(Glu_x$ -co-Ser_{1-x})₂₀₀, the fibril networks created by 398 $P(Glu_{0.65}-co-Ala_{0.3}-co-Val_{0.05})_{200}$ and $P(Glu_{0.7}-co-Ala_{0.2}-co-399)$ Val_{0.1})₂₀₀ featured a more rigid, with a "bush-like" branching 400 structure characterized by a high level of connectivity between 401 fibrils. The fibrils assembled from P(Glu_{0.65}-co-Ala_{0.3}-co- 402

403 Val_{0.05})₂₀₀ and P(Glu_{0.7}-co-Ala_{0.2}-co-Val_{0.1})₂₀₀ exhibited a 404 predominant β-sheet secondary structure with some coil 405 conformation, as revealed by FTIR and WAXD studies (Figure 406 S20 and S21). Observing that the filament density in the 407 P(Glu_{0.7}-co-Ala_{0.2}-co-Val_{0.1})₂₀₀ sample appeared to be higher 408 than that in P(Glu_{0.65}-co-Ala_{0.3}-co-Val_{0.05})₂₀₀, we prepared an 409 additional sample, P(Glu_{0.65}-co-Ala_{0.25}-co-Val_{0.1})₂₀₀. The mor-410 phology of its fibril network closely resembled that of P(Glu_{0.7}-411 co-Ala_{0.2}-co-Val_{0.1})₂₀₀, as shown in Figure S33. This similarity 412 indicates that the filament density in these hydrogel networks 413 is primarily influenced by the composition of Val.

Several factors may contribute to this unique superstructure to control: (1) The chain regularity was significantly disrupted by the inclusion of Ala and Val residues, preventing the pairwise tacking of β -sheet protofibrils into large spherulites that are prone to precipitation. (2) The introduction of Val facilitated rapid nucleation, while Ala effectively moderated the growth phase. This synergistic effect led to the formation of fibril bundles that predominantly assembled into branched fibril clusters, swiftly covering the entire sample space. (3) The hydrophobic attractions between the nonpolar residues fostered an increased network connectivity between the fibrils and fibril bundles.

Enhanced Mechanical Strength and Structural 427 Adaptability of Interlinked Fibril Cluster Hydrogels. In 428 comparison with entangled fibril hydrogels from P(Glu_{1-x}-co-429 Ser_x)₂₀₀, the hydrogel composed of P(Glu_{0.65}-co-Ala_{0.3}-co-430 Val_{0.05})₂₀₀ showed substantially greater strength, reaching a 431 G' of 600 Pa (Figure 5a and Figure S34a). This suggests 432 enhanced stability within the fibril cluster network. The higher 433 hydrophobicity of its amino acid constituents in P(Glu_{0.65}-co-434 Ala_{0.3}-co-Val_{0.05})₂₀₀ led to stronger chain interactions and 435 increased fibril connectivity, forming a more resilient filament 436 network. Interestingly, while the fibril superstructures of 437 hydrogel of P(Glu_{0.7}-co-Ala_{0.2}-co-Val_{0.1})₂₀₀ were significantly 438 thinner and denser than those of P(Glu_{0.65}-co-Ala_{0.3}-co-439 $Val_{0.05})_{200}$, their G' and strain-dependence were similar (Figure 440 5c and Figure S34b). However, the G'' of the P(Glu_{0.7}-co-441 Ala_{0.2}-co-Val_{0.1})₂₀₀ hydrogel was nearly double that of P-442 (Glu_{0.65}-co-Ala_{0.3}-co-Val_{0.05})₂₀₀. Despite their superior strength, 443 the networks of $P(Glu_{0.65}$ -co-Ala_{0.3}-co-Val_{0.05})₂₀₀ and $P(Glu_{0.7}$ -444 co-Ala_{0.2}-co-Val_{0.1})₂₀₀ maintained a self-healing capability 445 comparable to that of $P(Glu_{0.5}$ -co- $Ser_{0.5})_{200}$ when subjected 446 to large strains (Figure 5b,d).

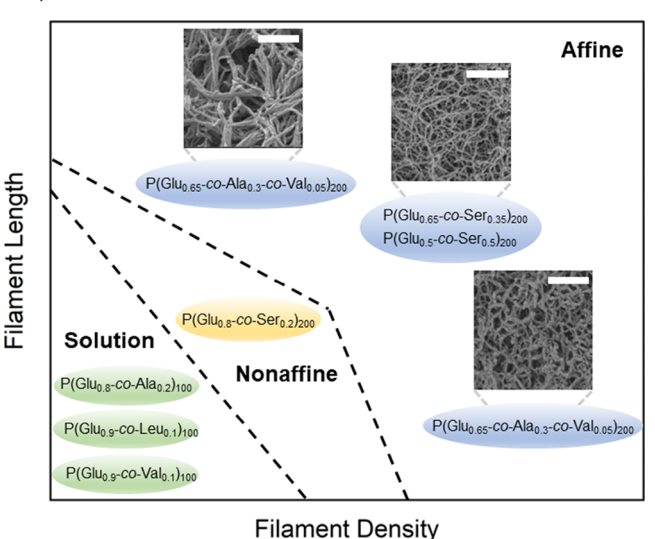
While the structural aspects in these fibril cluster gels might 448 resemble those found in some rod cluster gels formed in 449 colloidal assembly, 42 they are not premade building blocks 450 assembled later by depletion forces. Instead, the copolypeptides, functioning as supramolecular monomers, gradually evolved into an interconnected fibril cluster network. This 453 fibril nucleation and growth persist until the entire available 454 space is filled by the connected supramolecular network, 455 arresting the dynamics of individual fibrils or fibril clusters. 456 This gelation process is strongly governed by supramolecular 457 assembly kinetics, making them highly responsive to variations 458 in molecular designs. For example, with 5% Val percentage, 459 resulting filaments from P(Glu_{0.65}-co-Ala_{0.3}-co-Val_{0.05})₂₀₀ tend 460 to be elongated and thick, albeit at a reduced filament density. 461 In contrast, with 10% Val, enhanced nucleation amplifies 462 filament density, producing shorter, finer filaments in the 463 P(Glu_{0.7}-co-Ala_{0.2}-co-Val_{0.1})₂₀₀ hydrogel, given the same poly-464 peptide concentration. For filaments of a given range of 465 persistence lengths, the elasticity of semiflexible filament

networks is typically a function of filament length and 466 density. Longer filaments with lower densities might 467 emphasize the entropic stretching of filaments for elasticity. 468 Meanwhile, shorter, denser filaments might shift the network's 469 dominance to enthalpic bending and stretching. Our random 470 copolypeptides offer a diverse range of filament lengths, 471 densities, and connectivities, creating experimental model 472 systems to explore the physics of such networks.

General Design Concepts for Fibrous Networks 474 Derived from Synthetic Random Copolypeptides. 475 Macintosh and colleagues have previously developed a diagram 476 that illustrates how variations in the length and number density 477 of semiflexible filaments influence network elasticity. 15,77 This 478 diagram offers a clear depiction of the network behavior, 479 making it a valuable tool in guiding the experimental design of 480 a fibrous network. For example, short filaments at low densities 481 are insufficient for forming networks due to inadequate cross- 482 linking, which leaves the filaments in a solute state. Beyond a 483 certain threshold of density and length, a percolation network 484 forms, yet it may display nonaffine characteristics where local 485 regions deform independently of the overall macroscopic 486 deformation. In contrast, networks composed of long filaments 487 at low densities, or those with high densities but short 488 intercross-link filament lengths, tend to exhibit affine behavior. 489 Here, local deformations are coordinated with the macroscopic 490 strain, leading to distinctive elastic and mechanical properties. 491

In our study, the dynamics of filament network and the 492 nature of cross-links are also crucial, considering that the cross-493 links between filaments in supramolecular gels may be 494 transient. Yet qualitatively, the behaviors of fibrils or fibril 495 networks derived from specific copolypeptide compositions 496 align with the regions outlined in Scheme 2, conforming to the 497 s2

Scheme 2. Sketch Representation of a Diagram Categorizing Filamentous Assemblies or Networks Formed by Synthetic Copolypeptides with Specific Compositions (Scale Bar: 500 nm)



general trends of length and density dependence described by 498 the established theory. Although our findings are still in their 499 early stages, this dependence could inform the design of 500 copolypeptides for specific network architectures. It is 501 remarkable that our investigations, using a limited set of just 502 five amino acids, have yielded a diverse array of network 503

572

573

582

583

584

586

588

589

590

591

592

593

594

595

596

597

598

599

600

601

602

603

605

606

607

608

609

610

611

612

504 structures. Nevertheless, additional studies are necessary to 505 definitively categorize these structures within the distinct 506 regimes of affine or nonaffine networks, based on their elastic 507 responses and deformation modes—whether filaments pre-508 dominantly stretch and compress or bending modes prevail. 15 509 Furthermore, our hydrogel samples exhibited a broad spectrum 510 of storage and loss moduli, without relying on non-network 511 species, external modulators, or added cross-linkers. These 512 moduli values are comparable to those found in reconstituted 513 extracellular matrices (ECM), 7,14 e.g., G': 10–1000 Pa; G'': 514 1-100 Pa. We anticipate that the introduction of permanent 515 cross-links, such as by integrating a minor proportion of 516 cysteine (Cys) into the random copolypeptides, could 517 markedly enhance the modulus, bringing it closer to the 518 viscoelastic properties of soft tissues.

519 CONCLUSIONS

520 In summary, this study presents two novel strategies for the 521 design and synthesis of synthetic random copolypeptides with 522 the potential to self-assemble into biomimetic supramolecular 523 hydrogels. The first approach utilizes amino acids with polar 524 side chains, specifically serine, to develop copolypeptides that 525 can form stable filament networks with tunable viscoelastic 526 properties. The second strategy employs nonpolar amino acids, 527 specifically valine and alanine, harnessing their ability to steer 528 the architecture of fibrils, influencing their higher-order 529 superstructures and assembly kinetics and thus promoting 530 the creation of extensive networks. Both strategies yielded 531 supramolecular hydrogels characterized by a self-healing 532 capability, underscoring their potential suitability for bio-533 medical applications. Furthermore, this work sheds light on the 534 core principles steering the gelation pathways of synthetic 535 copolypeptides, enhancing our understanding of the intrinsic 536 processes that guide their self-assembling tendencies. Future 537 research could seek to broaden this knowledge base, exploring 538 diverse amino acid combinations and their synergistic actions 539 to refine the tunability of mechanical and other physical 540 properties in these synthetic filamentary networks.

ASSOCIATED CONTENT

542 Supporting Information

545

546

547

548

549

550

551

552

553

554

555

556

557

558

560

561

562

563

543 The Supporting Information is available free of charge at s44 https://pubs.acs.org/doi/10.1021/jacs.3c10762.

> Materials and methods; nuclear magnetic resonance (NMR); gel permeation chromatography (GPC); NCA copolymerization kinetics by high performance liquid chromatography (HPLC); circular dichroism (CD) spectra; Fourier transform infrared (FTIR) spectra; small-angle X-ray scattering (SAXS) and wide-angle Xray scattering (WAXS); ThT-based fluorescence kinetic assays by microplate reader; transmission electron microscopy (TEM) and negatively stained TEM; Scanning electron microscopy (SEM) and critical point dryer; rheology; experimental section; synthesis of Obenzyl-L-Serine NCA (BLS-NCA); synthesis of Obenzyl-L-tyrosine NCA (BLT-NCA); synthesis of copolypeptides with leucine, alanine, valine, and tyrosine; synthesis of copolypeptides with serine via SIMPLE polymerization method; synthesis of copolypeptides with three components with crown ether (CE) as catalyst; determination of the randomness of amino acids in the copolypeptides by NCA ROP copolymeriza

tion kinetics; supramolecular assembly of copolypeptides 564 in dilute solutions; supramolecular hydrogelation of 565 copolypeptides; supramolecular assembly kinetics of 566 copolypeptides monitored by in situ ThT fluorescence 567 assays; supramolecular assembly kinetic data processing; 568 analysis of the supramolecular assembly kinetics; 569 statistics of the length and width of supramolecular 570 assemblies (PDF)

AUTHOR INFORMATION

Corresponding Authors

Jianjun Cheng – Department of Chemistry and Department of 574 Materials Science and Engineering, University of Illinois at 575 Urbana-Champaign, Urbana, Illinois 61801, United States; 576 orcid.org/0000-0003-2561-9291; Email: jianjunc@ illinois.edu

Yao Lin - Polymer Program, Institute of Materials Science and 579 Department of Chemistry, University of Connecticut, Storrs, 580 Connecticut 06269, United States; o orcid.org/0000-0001-581 5227-2663; Email: yao.lin@uconn.edu

Authors

Tianjian Yang – Polymer Program, Institute of Materials Science, University of Connecticut, Storrs, Connecticut 06269, 585 United States

Tianrui Xue - Department of Chemistry, University of Illinois 587 at Urbana-Champaign, Urbana, Illinois 61801, United

Jianan Mao - Department of Chemistry, University of Connecticut, Storrs, Connecticut 06269, United States

Yingying Chen - Department of Materials Science and Engineering, University of Illinois at Urbana-Champaign, Urbana, Illinois 61801, United States

Huidi Tian - Department of Chemistry, University of Connecticut, Storrs, Connecticut 06269, United States Arlene Bartolome - Department of Chemistry, University of

Connecticut, Storrs, Connecticut 06269, United States Hongwei Xia - Department of Chemistry, University of Connecticut, Storrs, Connecticut 06269, United States

Xudong Yao - Department of Chemistry, University of Connecticut, Storrs, Connecticut 06269, United States

Challa V. Kumar - Department of Chemistry, University of Connecticut, Storrs, Connecticut 06269, United States; orcid.org/0000-0002-4396-8738

Complete contact information is available at: https://pubs.acs.org/10.1021/jacs.3c10762

Author Contributions

 $^{\perp}$ T.Y. and T.X. contributed equally to this work.

ı

The authors declare no competing financial interest.

ACKNOWLEDGMENTS

This work was supported by the NSF grant (DMR 1809497 613 and DMR 2210590 to Y.L.; CHE-1905097 to J.C.). The 614 authors thank Dr. Xuanhao Sun at the UConn Bioscience 615 Electron Microscopy Lab for instrument training, Prof. Anson 616 Ma at the UConn Polymer Program for comments and 617 suggestions, and Dr. Lin Yang at the Brookhaven National Lab 618 for assistance with WAXD studies. The LiX beamline is part of 619 the Center for BioMolecular Structure (CBMS), which is 620 primarily supported by the National Institutes of Health, 621

622 National Institute of General Medical Sciences (NIGMS) 623 through a P30 Grant (P30GM133893), and by the DOE 624 Office of Biological and Environmental Research 625 (KP1605010). LiX also received additional support from 626 NIH Grant S10 OD012331. As part of NSLS-II, a national user 627 facility at Brookhaven National Laboratory, work performed at 628 the CBMS is supported in part by the U.S. Department of 629 Energy, Office of Science, Office of Basic Energy Sciences 630 Program under contract number DE-SC0012704.

631 REFERENCES

- 632 (1) Oosawa, F.; Asakura, S. Thermodynamics of the Polymerization of 633 Protein; Academic Press, 1975.
- 634 (2) Fletcher, D. A.; Mullins, R. D. Cell mechanics and the 635 cytoskeleton. *Nature* **2010**, 463, 485–492.
- 636 (3) Pollard, T. D.; Borisy, G. G. Cellular motility driven by assembly 637 and disassembly of actin filaments. *Cell* **2003**, *112*, 453–465.
- 638 (4) Goodwin, S. S.; Vale, R. D. Patronin regulates the microtubule 639 network by protecting microtubule minus ends. *Cell* **2010**, *143*, 263–640 274.
- 641 (5) Yurchenco, P. D.; Ruben, G. C. Basement membrane structure 642 in situ: evidence for lateral associations in the type IV collagen 643 network. *J. Cell Biol.* 1987, 105, 2559–2568.
- 644 (6) Ottani, V.; Raspanti, M.; Ruggeri, A. Collagen structure and 645 functional implications. *Micron* **2001**, *32*, 251–260.
- 646 (7) Storm, C.; Pastore, J. J.; MacKintosh, F. C.; Lubensky, T. C.; 647 Janmey, P. A. Nonlinear elasticity in biological gels. *Nature* **2005**, 435, 648 191–194.
- 649 (8) Gardel, M.; Shin, J. H.; MacKintosh, F.; Mahadevan, L.; 650 Matsudaira, P.; Weitz, D. A. Elastic behavior of cross-linked and 651 bundled actin networks. *Science* **2004**, *304*, 1301–1305.
- 652 (9) Lin, Y.-C.; Koenderink, G. H.; MacKintosh, F. C.; Weitz, D. A. 653 Viscoelastic properties of microtubule networks. *Macromolecules* **2007**, 654 40, 7714–7720.
- 655 (10) Forgacs, G.; Newman, S. A.; Hinner, B.; Maier, C. W.; 656 Sackmann, E. Assembly of collagen matrices as a phase transition 657 revealed by structural and rheologic studies. *Biophys. J.* **2003**, *84*, 658 1272–1280.
- 659 (11) Licup, A. J.; Münster, S.; Sharma, A.; Sheinman, M.; Jawerth, L. 660 M.; Fabry, B.; Weitz, D. A.; MacKintosh, F. C. Stress controls the 661 mechanics of collagen networks. *Proc. Natl. Acad. Sci. U. S. A.* 2015, 662 112, 9573–9578.
- 663 (12) Fratzl, P.; Misof, K.; Zizak, I.; Rapp, G.; Amenitsch, H.; 664 Bernstorff, S. Fibrillar structure and mechanical properties of collagen. 665 *J. Struct. Biol.* **1998**, *122*, 119–122.
- 666 (13) Moeendarbary, E.; Valon, L.; Fritzsche, M.; Harris, A. R.; 667 Moulding, D. A.; Thrasher, A. J.; Stride, E.; Mahadevan, L.; Charras, 668 G. T. The cytoplasm of living cells behaves as a poroelastic material. 669 *Nat. Mater.* **2013**, *12*, 253–261.
- 670 (14) Chaudhuri, O.; Cooper-White, J.; Janmey, P. A.; Mooney, D. J.; 671 Shenoy, V. B. Effects of extracellular matrix viscoelasticity on cellular 672 behaviour. *Nature* **2020**, *584*, 535–546.
- 673 (15) Pritchard, R. H.; Huang, Y. Y. S.; Terentjev, E. M. Mechanics of 674 biological networks: from the cell cytoskeleton to connective tissue. 675 *Soft Matter* **2014**, *10*, 1864–1884.
- 676 (16) Yokoi, H.; Kinoshita, T.; Zhang, S. Dynamic reassembly of 677 peptide RADA16 nanofiber scaffold. *Proc. Natl. Acad. Sci. U. S. A.* 678 **2005**, 102, 8414–8419.
- 679 (17) Li, X.; Kuang, Y.; Lin, H. C.; Gao, Y.; Shi, J.; Xu, B. 680 Supramolecular nanofibers and hydrogels of nucleopeptides. *Angew*. 681 *Chem., Int. Ed.* **2011**, *50*, 9365–9369.
- 682 (18) Freeman, R.; Han, M.; Alvarez, Z.; Lewis, J. A.; Wester, J. R.; 683 Stephanopoulos, N.; McClendon, M. T.; Lynsky, C.; Godbe, J. M.; 684 Sangji, H.; Luijten, E.; Stupp, S. I. Reversible self-assembly of 685 superstructured networks. *Science* **2018**, 362, 808–813.
- 686 (19) Kouwer, P. H.; Koepf, M.; Le Sage, V. A.; Jaspers, M.; Van 687 Buul, A. M.; Eksteen-Akeroyd, Z. H.; Woltinge, T.; Schwartz, E.; 688 Kitto, H. J.; Hoogenboom, R.; Picken, S. J.; Nolte, R. J. M.; Mendes,

- E.; Rowan, A. E. Responsive biomimetic networks from polyisocya- 689 nopeptide hydrogels. *Nature* **2013**, 493, 651–655.
- (20) O'leary, L. E.; Fallas, J. A.; Bakota, E. L.; Kang, M. K.; 691 Hartgerink, J. D. Multi-hierarchical self-assembly of a collagen 692 mimetic peptide from triple helix to nanofibre and hydrogel. *Nat.* 693 *Chem.* 2011, 3, 821–828.
- (21) Wang, F.; Su, H.; Xu, D.; Dai, W.; Zhang, W.; Wang, Z.; 695 Anderson, C. F.; Zheng, M.; Oh, R.; Wan, F.; Cui, H. Tumour 696 sensitization via the extended intratumoural release of a STING 697 agonist and camptothecin from a self-assembled hydrogel. *Nat.* 698 *Biomed. Eng.* 2020, 4, 1090–1101.
- (22) Diba, M.; Spaans, S.; Hendrikse, S. I. S.; Bastings, M. M. C.; 700 Schotman, M. J. G.; van Sprang, J. F.; Wu, D. J.; Hoeben, F. J. M.; 701 Janssen, H. M.; Dankers, P. Y. W. Engineering the dynamics of cell 702 adhesion cues in supramolecular hydrogels for facile control over cell 703 encapsulation and behavior. *Adv. Mater.* **2021**, *33*, 2008111.
- (23) Chivers, P. R.; Smith, D. K. Shaping and structuring 705 supramolecular gels. *Nat. Rev. Mater.* **2019**, *4*, 463–478.
- (24) Gelain, F.; Luo, Z.; Zhang, S. Self-assembling peptide EAK16 707 and RADA16 nanofiber scaffold hydrogel. *Chem. Rev.* **2020**, *120*, 708 13434–13460.
- (25) Petka, W. A.; Harden, J. L.; McGrath, K. P.; Wirtz, D.; Tirrell, 710 D. A. Reversible hydrogels from self-assembling artificial proteins. 711 Science 1998, 281, 389–392.
- (26) van Hest, J. C.; Tirrell, D. A. Protein-based materials, toward a 713 new level of structural control. *Chem. Commun.* **2001**, 1897–1904. 714
- (27) Vepari, C.; Kaplan, D. L. Silk as a biomaterial. *Prog. Polym. Sci.* 715 **2007**, 32, 991–1007.
- (28) Levin, A.; Hakala, T. A.; Schnaider, L.; Bernardes, G. J. L.; 717 Gazit, E.; Knowles, T. P. J. Biomimetic peptide self-assembly for 718 functional materials. *Nat. Rev. Chem.* **2020**, *4*, 615–634.
- (29) Deng, C.; Wu, J.; Cheng, R.; Meng, F.; Klok, H.-A.; Zhong, Z. $_{720}$ Functional polypeptide and hybrid materials: Precision synthesis via $_{721}$ α -amino acid N-carboxyanhydride polymerization and emerging $_{722}$ biomedical applications. *Prog. Polym. Sci.* **2014**, *39*, 330–364.
- (30) Deming, T. J. Synthetic polypeptides for biomedical 724 applications. *Prog. Polym. Sci.* **2007**, 32, 858–875.
- (31) Hadjichristidis, N.; Iatrou, H.; Pitsikalis, M.; Sakellariou, G. 726 Synthesis of well-defined polypeptide-based materials via the ring- 727 opening polymerization of α -amino acid N-carboxyanhydrides. *Chem.* 728 *Rev.* 2009, 109, 5528–5578.
- (32) Deming, T. J. Synthesis of side-chain modified polypeptides. 730 *Chem. Rev.* **2016**, *116*, 786–808.
- (33) Lu, H.; Wang, J.; Song, Z.; Yin, L.; Zhang, Y.; Tang, H.; Tu, C.; 732 Lin, Y.; Cheng, J. Recent advances in amino acid N-carboxyanhy- 733 drides and synthetic polypeptides: chemistry, self-assembly and 734 biological applications. *Chem. Commun.* **2014**, *50*, 139–155.
- (34) Rodriguez-Hernandez, J.; Chécot, F.; Gnanou, Y.; 736 Lecommandoux, S. Toward 'smart'nano-objects by self-assembly of 737 block copolymers in solution. *Prog. Polym. Sci.* **2005**, *30*, 691–724. 738
- (35) Chen, S.; Berthelier, V.; Hamilton, J. B.; O'Nuallai, B.; Wetzel, 739 R. Amyloid-like features of polyglutamine aggregates and their 740 assembly kinetics. *Biochem.* **2002**, *41*, 7391–7399.
- (36) Fändrich, M.; Dobson, C. M. The behaviour of polyamino acids 742 reveals an inverse side chain effect in amyloid structure formation. 743 *EMBO J.* **2002**, 21, 5682–5690. 744
- (37) Yang, T.; Benson, K.; Fu, H.; Xue, T.; Song, Z.; Duan, H.; Xia, 745 H.; Kalluri, A.; He, J.; Cheng, J.; Kumar, C. V.; Lin, Y. Modeling and 746 Designing Particle-Regulated Amyloid-like Assembly of Synthetic 747 Polypeptides in Aqueous Solution. *Biomacromolecules* **2021**, 23, 196–748 209.
- (38) Colaco, M.; Park, J.; Blanch, H. The kinetics of aggregation of 750 poly-glutamic acid based polypeptides. *Biophys. Chem.* **2008**, 136, 74–751 86.
- (39) Du, X.; Zhou, J.; Shi, J.; Xu, B. Supramolecular hydrogelators 753 and hydrogels: from soft matter to molecular biomaterials. *Chem. Rev.* 754 **2015**, *115*, 13165–13307.

- 756 (40) Goor, O. J.; Hendrikse, S. I.; Dankers, P. Y.; Meijer, E. From 757 supramolecular polymers to multi-component biomaterials. *Chem.* 758 Soc. Rev. **2017**, 46, 6621–6637.
- 759 (41) Mohraz, A.; Solomon, M. J. Gelation and internal dynamics of 760 colloidal rod aggregates. *J. Colloid Interface Sci.* **2006**, 300, 155–162.
- 761 (42) Wilkins, G. M.; Spicer, P. T.; Solomon, M. J. Colloidal system 762 to explore structural and dynamical transitions in rod networks, gels, 763 and glasses. *Langmuir* **2009**, 25, 8951–8959.
- 764 (43) Meakin, P. Fractals, scaling and growth far from equilibrium; 765 Cambridge University Press, 1998.
- 766 (44) Trappe, V.; Prasad, V.; Cipelletti, L.; Segre, P.; Weitz, D. A. 767 Jamming phase diagram for attractive particles. *Nature* **2001**, *411*, 768 772–775.
- 769 (45) Solomon, M. J.; Spicer, P. T. Microstructural regimes of 770 colloidal rod suspensions, gels, and glasses. *Soft Matter* **2010**, *6*, 771 1391–1400.
- 772 (46) Su, L.; Mosquera, J.; Mabesoone, M. F.; Schoenmakers, S. M.; 773 Muller, C.; Vleugels, M. E.; Dhiman, S.; Wijker, S.; Palmans, A. R.; 774 Meijer, E. Dilution-induced gel-sol-gel-sol transitions by competitive 775 supramolecular pathways in water. *Science* **2022**, 377, 213–218.
- 776 (47) Pashuck, E. T.; Cui, H.; Stupp, S. I. Tuning supramolecular 777 rigidity of peptide fibers through molecular structure. *J. Am. Chem.* 778 Soc. **2010**, 132, 6041–6046.
- 779 (48) Edelbrock, A. N.; Clemons, T. D.; Chin, S. M.; Roan, J. J. W.; 780 Bruckner, E. P.; Álvarez, Z.; Edelbrock, J. F.; Wek, K. S.; Stupp, S. I. 781 Superstructured Biomaterials Formed by Exchange Dynamics and 782 Host—Guest Interactions in Supramolecular Polymers. *Adv. Sci.* 2021, 783 8, No. 2004042.
- 784 (49) Xia, H.; Fu, H.; Zhang, Y.; Shih, K.-C.; Ren, Y.; Anuganti, M.; 785 Nieh, M.-P.; Cheng, J.; Lin, Y. Supramolecular assembly of comb-like 786 macromolecules induced by chemical reactions that modulate the 787 macromolecular interactions in situ. *J. Am. Chem. Soc.* **2017**, *139*, 788 11106—11116.
- 789 (50) Link, A. J.; Mock, M. L.; Tirrell, D. A. Non-canonical amino 790 acids in protein engineering. *Curr. Opin. Biotechnol.* **2003**, *14*, 603–791 609.
- 792 (51) Liu, C. C.; Schultz, P. G. Adding new chemistries to the genetic 793 code. *Annu. Rev. Biochem.* **2010**, *79*, 413–444.
- 794 (52) Baumgartner, R.; Fu, H.; Song, Z.; Lin, Y.; Cheng, J. 795 Cooperative polymerization of α -helices induced by macromolecular 796 architecture. *Nat. Chem.* **2017**, *9*, 614–622.
- 797 (53) Song, Z.; Fu, H.; Wang, J.; Hui, J.; Xue, T.; Pacheco, L. A.; Yan, 798 H.; Baumgartner, R.; Wang, Z.; Xia, Y.; Wang, X.; Yin, L.; Chen, C.; 799 Rodríguez-López, J.; Ferguson, A. L.; Lin, Y.; Cheng, J. Synthesis of 800 polypeptides via bioinspired polymerization of in situ purified N-801 carboxyanhydrides. *Proc. Natl. Acad. Sci. U. S. A.* **2019**, *116*, 10658–802 10663.
- 803 (54) Wang, W.; Fu, H.; Lin, Y.; Cheng, J.; Song, Z. Cooperative 804 Covalent Polymerization of N-carboxyanhydrides: from Kinetic 805 Studies to Efficient Synthesis of Polypeptide Materials. *Acc. Chem.* 806 *Res.* 2023, 4, 604–615.
- 807 (55) Canning, A.; Pasquazi, A.; Fijten, M.; Rajput, S.; Buttery, L.; 808 Aylott, J. W.; Zelzer, M. Tuning the conformation of synthetic co-809 polypeptides of serine and glutamic acid through control over 810 polymer composition. *J. Polym. Sci., Part A: Polym. Chem.* **2016**, 54, 811 2331–2336.
- 812 (56) Gibson, M. I.; Cameron, N. R. Organogelation of sheet—helix 813 diblock copolypeptides. *Angew. Chem., Int. Ed.* **2008**, *120*, 5238–5240.
- 814 (57) Fan, J.; Zou, J.; He, X.; Zhang, F.; Zhang, S.; Raymond, J. E.; 815 Wooley, K. L. Tunable mechano-responsive organogels by ring-
- 816 opening copolymerizations of N-carboxyanhydrides. *Chem. Sci.* **2014**, 817 5, 141–150.
- 818 (58) Nisal, R.; Jayakannan, M. Tertiary-Butylbenzene Functionaliza-819 tion as a Strategy for β -Sheet Polypeptides. *Biomacromolecules* **2022**, 820 23, 2667–2684.
- 821 (S9) Xue, T.; Song, Z.; Wang, Y.; Zhu, B.; Zhao, Z.; Tan, Z.; Wang, 822 X.; Xia, Y.; Cheng, J. Streamlined synthesis of PEG-polypeptides
- 823 directly from amino acids. Macromolecules 2020, 53, 6589-6597.

- (60) Lu, H.; Cheng, J. Hexamethyldisilazane-mediated controlled 824 polymerization of α -amino acid N-carboxyanhydrides. J. Am. Chem. 825 Soc. 2007, 129, 14114–14115.
- (61) Song, Z.; Fu, H.; Baumgartner, R.; Zhu, L.; Shih, K.-C.; Xia, Y.; 827 Zheng, X.; Yin, L.; Chipot, C.; Lin, Y.; Cheng, J. Enzyme-mimetic self-828 catalyzed polymerization of polypeptide helices. *Nat. Commun.* **2019**, 829 10, 5470.
- (62) Fu, H.; Baumgartner, R.; Song, Z.; Chen, C.; Cheng, J.; Lin, Y. 831 Generalized model of cooperative covalent polymerization: connect- 832 ing the supramolecular binding interactions with the catalytic 833 behavior. *Macromolecules* **2022**, *55*, 2041–2050.
- (63) Xia, Y.; Song, Z.; Tan, Z.; Xue, T.; Wei, S.; Zhu, L.; Yang, Y.; 835 Fu, H.; Jiang, Y.; Lin, Y.; Lu, Y.; Ferguson, A. L.; Cheng, J. 836 Accelerated polymerization of N-carboxyanhydrides catalyzed by 837 crown ether. *Nat. Commun.* **2021**, *12*, 732.
- (64) Wang, J.; Lu, H.; Kamat, R.; Pingali, S. V.; Urban, V. S.; Cheng, 839 J.; Lin, Y. Supramolecular polymerization from polypeptide-grafted 840 comb polymers. *J. Am. Chem. Soc.* **2011**, *133*, 12906–12909.
- (65) Quadrifoglio, F.; Urry, D. Ultraviolet rotatory properties of 842 polypeptides in solution. II. Poly-L-serine. *J. Am. Chem. Soc.* **1968**, 90, 843 2760–2765.
- (66) Koenig, J.; Sutton, P. Raman scattering of some synthetic 845 polypeptides: Poly (γ -benzyl L-glutamate), poly-L-leucine, poly-L- 846 valine, and poly-L-serine. *Biopolymers* **1971**, *10*, 89–106.
- (67) Minor, D. L., Jr; Kim, P. S. Measurement of the β -sheet- 848 forming propensities of amino acids. *Nature* **1994**, 367, 660–663. 849
- (68) Levitt, M. Conformational preferences of amino acids in 850 globular proteins. *Biochem.* **1978**, *17*, 4277–4285.
- (69) Sereda, T. J.; Mant, C. T.; Sönnichsen, F. D.; Hodges, R. S. 852 Reversed-phase chromatography of synthetic amphipathic α -helical 853 peptides as a model for ligand/receptor interactions Effect of 854 changing hydrophobic environment on the relative hydrophilicity/ 855 hydrophobicity of amino acid side-chains. *J. Chromatogr. A* **1994**, 676, 856 139–153.
- (70) Naiki, H.; Higuchi, K.; Hosokawa, M.; Takeda, T. Fluorometric 858 determination of amyloid fibrils in vitro using the fluorescent dye, 859 thioflavine T. *Anal. Biochem.* **1989**, 177, 244–249.
- (71) Kricheldorf, H. R.; von Lossow, C.; Schwarz, G. Primary 861 Amine-Initiated Polymerizations of Alanine-NCA and Sarcosine- 862 NCA. *Macromol. Chem. Phys.* **2004**, 205, 918–924.
- (72) Bamford, C. H. Synthetic Polypeptides: Preparation, Structure, 864 and Properties; Academic Press, 1956.
- (73) Bishop, M. F.; Ferrone, F. A. Kinetics of nucleation-controlled 866 polymerization. A perturbation treatment for use with a secondary 867 pathway. *Biophys. J.* **1984**, *46*, 631–644.
- (74) Dear, A. J.; Meisl, G.; Michaels, T. C. T.; Zimmermann, M. R.; 869 Linse, S.; Knowles, T. P. J. The catalytic nature of protein aggregation. 870 J. Chem. Phys. 2020, 152, No. 045101.
- (75) Cohen, S. I.; Linse, S.; Luheshi, L. M.; Hellstrand, E.; White, D. 872 A.; Rajah, L.; Otzen, D. E.; Vendruscolo, M.; Dobson, C. M.; 873 Knowles, T. P. Proliferation of amyloid-β42 aggregates occurs through 874 a secondary nucleation mechanism. *Proc. Natl. Acad. Sci. U. S. A.* 875 **2013**, 110, 9758–9763.
- (76) Meisl, G.; Kirkegaard, J. B.; Arosio, P.; Michaels, T. C.; 877 Vendruscolo, M.; Dobson, C. M.; Linse, S.; Knowles, T. P. Molecular 878 mechanisms of protein aggregation from global fitting of kinetic 879 models. *Nat. Protoc.* **2016**, *11*, 252–272.
- (77) Head, D.; Levine, A.; MacKintosh, F. Distinct regimes of elastic 881 response and deformation modes of cross-linked cytoskeletal and 882 semiflexible polymer networks. *Phys. Rev. E* **2003**, *68*, No. 061907. 883